JCI insight

Transcriptional analysis of Foxp3$^+$ Tregs and functions of two identified molecules during resolution of ALI

Jason R. Mock, Catherine F. Dial, Miriya K. Tune, Dustin L. Norton, Jessica R. Martin, John C. Gomez, Robert S. Hagan, Hong Dang, Claire M. Doerschuk

JCI Insight. 2019;4(6):e124958. https://doi.org/10.1172/jci.insight.124958.

Research Article **Immunology** **Pulmonology**

Recovery from acute lung injury (ALI) is an active process. Foxp3$^+$ Tregs contribute to recovery from ALI through modulating immune responses and enhancing alveolar epithelial proliferation and tissue repair. The current study investigates Treg transcriptional profiles during resolution of ALI in mice. Tregs from either lung or splenic tissue were isolated from uninjured mice or mice recovering from ALI and then examined for differential gene expression between these conditions. In mice with ALI, Tregs isolated from the lungs had hundreds of differentially expressed transcripts compared with those from the spleen, indicating that organ specificity and microenvironment are critical in Treg function. These regulated transcripts suggest which intracellular signaling pathways modulate Treg behavior. Interestingly, several transcripts having no prior recognized function in Tregs were differentially expressed by lung Tregs during resolution. Further investigation into 2 identified transcripts, *Mmp12* and *Sik1*, revealed that Treg-specific expression of each plays a role in Treg-promoted ALI resolution. This study provides potentially novel information describing the signals that may expand resident Tregs, recruit or retain them to the lung during ALI, and modulate their function. The results provide insight into both tissue- and immune microenvironment–specific transcriptional differences through which Tregs direct their effects.

JCI insight

RESEARCH ARTICLE

Transcriptional analysis of Foxp3$^+$ Tregs and functions of two identified molecules during resolution of ALI

Jason R. Mock,[1,2] Catherine F. Dial,[1,2] Miriya K. Tune,[1,2] Dustin L. Norton,[1,2] Jessica R. Martin,[2,3] John C. Gomez,[2,3] Robert S. Hagan,[1,2] Hong Dang,[2] and Claire M. Doerschuk[1,2,3]

[1]Division of Pulmonary Diseases and Critical Care Medicine, Department of Medicine, [2]Marsico Lung Institute, and [3]Center for Airways Disease, University of North Carolina (UNC), Chapel Hill, North Carolina, USA.

Recovery from acute lung injury (ALI) is an active process. Foxp3$^+$ Tregs contribute to recovery from ALI through modulating immune responses and enhancing alveolar epithelial proliferation and tissue repair. The current study investigates Treg transcriptional profiles during resolution of ALI in mice. Tregs from either lung or splenic tissue were isolated from uninjured mice or mice recovering from ALI and then examined for differential gene expression between these conditions. In mice with ALI, Tregs isolated from the lungs had hundreds of differentially expressed transcripts compared with those from the spleen, indicating that organ specificity and microenvironment are critical in Treg function. These regulated transcripts suggest which intracellular signaling pathways modulate Treg behavior. Interestingly, several transcripts having no prior recognized function in Tregs were differentially expressed by lung Tregs during resolution. Further investigation into 2 identified transcripts, *Mmp12* and *Sik1*, revealed that Treg-specific expression of each plays a role in Treg-promoted ALI resolution. This study provides potentially novel information describing the signals that may expand resident Tregs, recruit or retain them to the lung during ALI, and modulate their function. The results provide insight into both tissue- and immune microenvironment–specific transcriptional differences through which Tregs direct their effects.

Introduction

Acute events such as pneumonia, inhalational injury, trauma, or sepsis often damage the lung epithelium, which consequently can impede the primary function of the lung exchanging oxygen and carbon dioxide. Repair of the epithelium after injury is necessary to restore homeostasis, and current views propose that the immune system plays an important role in enhancing barrier function and promoting resolution (1–4). Resolution is an actively regulated program involving clearance of edema fluid, removal of apoptotic cells, matrix remodeling, and repair of alveolar epithelium (4–8). The mechanisms underlying the resolution process are not well characterized (2).

Foxp3$^+$ Tregs are a distinct population of CD4$^+$ lymphocytes, identified by their expression of the transcription factor Forkhead homeobox protein-3 (FOXP3). This population suppresses and downregulates immune responses in allergic and autoimmune diseases (9, 10).

Tregs serve a central role in suppressing the immune response and facilitating resolution in experimental acute lung injury (ALI) (11, 12). They contribute to tissue repair through the expression of the growth factor amphiregulin (AREG) (13, 14). Patients with acute respiratory distress syndrome (ARDS) have increased numbers of Tregs in the bronchoalveolar compartment (12, 15). Our prior studies demonstrate that Tregs enhance alveolar epithelial proliferation after injury in vivo and that Tregs directly promote AT2 proliferation in vitro, in part by a contact-independent mechanism, through the expression of keratinocyte growth factor (KGF) (16). However, the mechanisms by which Tregs facilitate resolution are far from clear and likely dependent on the type of injury, the microenvironment, and the target cells in question. In the study presented here, we sought to identify potential differences in lung-specific Treg transcript expression profiles during a time of resolution from lung injury, as compared with Tregs from uninjured lungs and with Tregs obtained from another tissue site (splenic Tregs) during resolution.

Submitted: September 18, 2018
Accepted: February 5, 2019
Published: March 21, 2019.

Reference information: *JCI Insight.* 2019;4(6):e124958. https://doi.org/10.1172/jci.insight.124958.

The established lung injury model of intratracheal LPS–induced (i.t. LPS–induced) injury, which has been well characterized for eliciting alveolar epithelial damage and a neutrophilic influx, elicits a very reproducible inflammatory response (11, 17, 18). Moreover, i.t. LPS administration at this dosage is followed by a consistent and uniform resolution process (11). Therefore, this model is well suited for studying transcriptional changes when studies require a combination of multiple samples to obtain adequate numbers for downstream analysis.

Data herein demonstrate that, during ALI resolution, Tregs regulate their expression of genes such as *Areg*, *Ctla4*, *Icos*, *Il10, Itgae*, and *Sgk1*, known to be important for their function in immune suppression or tissue repair (11, 13, 19–21). Several chemokines, cytokines, and chemokine and cytokine receptors were also differentially expressed, including *Cxcl16*, *Ccr5*, *Ccr2*, *Cxcr4*, *Cxcr5*, *Cxcr6*, *Ifngr2*, *Il1rl1*, and *Il18r1*. These observations provide insight into the signals that may expand resident Tregs, recruit them from distant sites or retain them in the lung during ALI. Interestingly, other transcripts such as *C3ar1*, *C5ar1*, *Mmp12*, and *Sik1,* which have little to no known role in Treg function, were differentially expressed during resolution of injury. Studies pursuing the expression and function of MMP12 show that Treg-expressed MMP12 may either minimize the recruitment of neutrophils or facilitate their clearance. Additional investigation into the function of SIK1 in Tregs demonstrates that absence of *Sik1* affects Treg number and their expression of the integrin CD103 (αEβ7) during ALI resolution.

These studies provide insight into both the tissue- and immune microenvironment–specific transcriptional responses by which Tregs direct their suppressive and tissue-reparative effects during resolution of experimental ALI. Our results underline the complexity of Treg function in the processes of tissue repair following lung injury.

Results

Treg population increases in the lung during resolution of LPS-induced ALI. Previous reports demonstrate that Treg expansion in the lung peaks at 7 days after injury in this LPS model of ALI in mice (11, 12). To quantify the change in the number of Tregs before and during the resolution phase of injury, we employed *Foxp3*^{EGFP} mice, in which the gene for enhanced GFP (EGFP) was inserted downstream of the endogenous *Foxp3* locus, resulting in fluorescence of all Foxp3-expressing cells (22).

The data show that, by day 7 after injury, male mice exposed to LPS have begun to recover from their weight loss due to the injury, which nadirs at day 4 after LPS (Figure 1A). Total lung cell count in the enzymatically digested single cell suspensions, total bronchoalveolar lavage (BAL) cell numbers, and BAL total protein concentration at days 7 and 10 after injury remain elevated compared with uninjured control mice (Figure 1, B–D) (11). The number of Foxp3$^+$ cells was determined in both the bronchoalveolar space and in single cell suspensions generated from whole lung digests following lung lavage (Figure 1, E and F). The number of lavageable Tregs in the airspace increases significantly at days 7 and 10 (Figure 1E). In the lung digests made following lavage, the number of Tregs increases approximately 3.7-fold (Figure 1F) during ALI resolution at day 7 after injury, and by 10 days, the numbers begin to trend downward, similar to a prior report utilizing a different *Foxp3* reporter strain (11). Comparison of Figure 1E with Figure 1F demonstrates that almost all (>99%) of the lung Tregs are present in the lung digest and not lavageable. The percentage of Foxp3$^+$ cells within the total CD4$^+$ cell population also increases during resolution at days 7 and 10 after injury in the lung cell suspensions (Figure 1G). These observations demonstrate that Tregs are present in uninjured lungs, increase within both the lavageable alveolar space and the lung parenchyma during ALI resolution, and peak at 7 days after LPS in this Treg transgenic reporter mouse line, similarly to WT mice (11).

Lung and spleen Tregs have distinct transcriptomes during ALI resolution. To determine potential changes in Treg transcriptional expression during experimental ALI, we performed transcriptome profiling of sorted Tregs. Three sets of Tregs were examined: (a) Lung Tregs sorted from uninjured lungs (control lung Tregs), (b) lung Tregs sorted at 7 days after LPS injury (resolving lung Tregs), and (c) splenic Tregs sorted at 7 days after LPS injury (resolving splenic Tregs) from the same mice as the resolving lung Tregs. To obtain adequate numbers of Tregs for mRNA analysis, combining single cell suspensions from multiple mice was required before sorting for each condition and replicate (n = 15–27 mice/experimental replicate). This study utilized both male and female mice age 8–12 weeks, and 3 replicates were performed for each of the 3 conditions. The gating scheme and postsorting percentages are shown in Supplemental Figure 1 (supplemental material available online with this article; https://doi.org/10.1172/jci.insight.124958DS1). The purity of the Treg sets was greater than 93% after cell sorting. The mortality

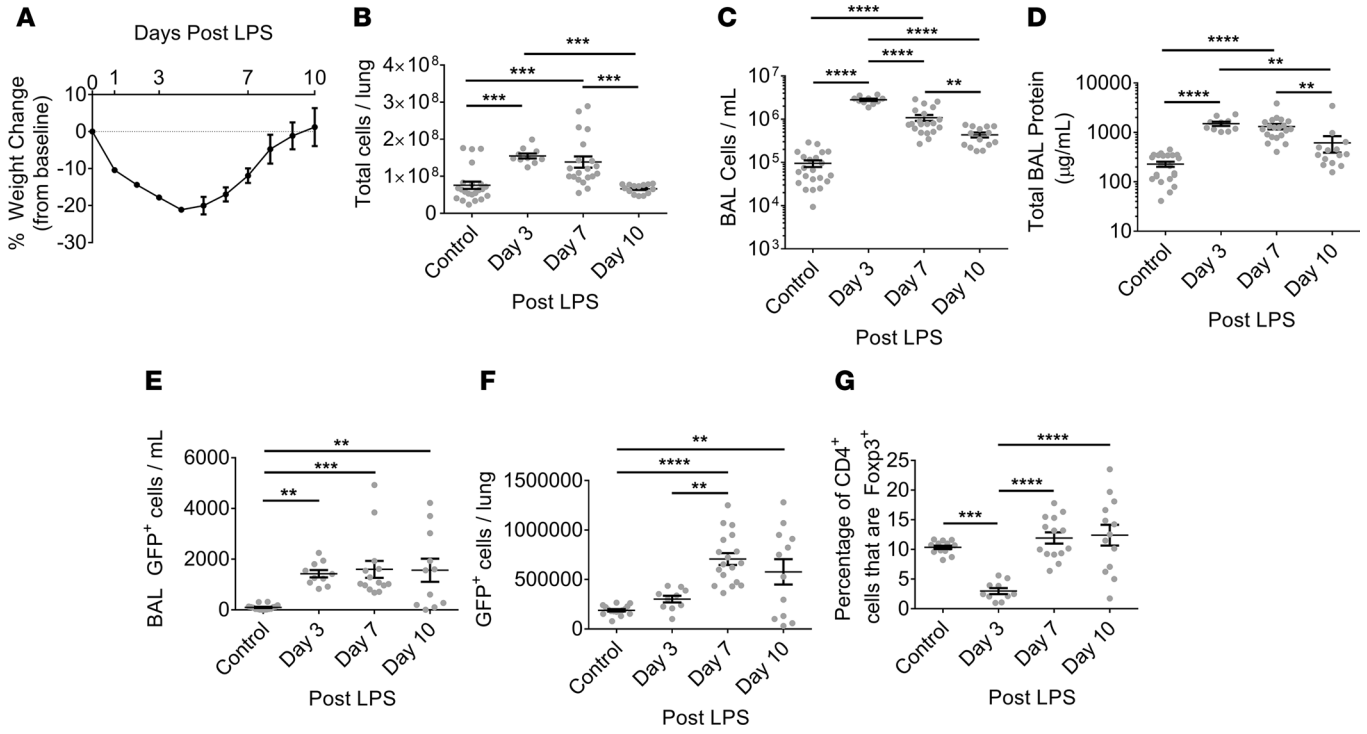

Figure 1. Foxp3⁺ Tregs increase in the lung during resolution of ALI. Male *Foxp3*^{EGFP} mice were challenged with LPS (3 mg/kg) intratracheally. (**A**) Body weight relative to baseline measured daily before and after injury (n = 15–47 per time point). (**B–D**) Total lung cell count in the lung digest (**B**), total cell counts in the bronchoalveolar lavage (BAL) (**C**), and BAL total protein concentration (**D**) were determined in *Foxp3*^{EGP} mice, either unchallenged or after treatment with LPS (n = 10–22 per time point; combined from 2–3 separate experiments). (**E–F**) The number of GFP⁺ cells in the BAL (**E**) or lung digests (**F**) of unchallenged mice and mice 3, 7, or 10 days after LPS (n = 10–16 per condition). (**G**) The percentage of total CD4⁺ cells that were Foxp3⁺, determined in unchallenged mice or mice 3, 7, or 10 days after LPS (n = 10–16 per condition). Data are expressed as the mean ± SEM where applicable. P values were determined by 1-way ANOVA with Tukey's multiple comparison test between conditions. $^{**}P < 0.01$ $^{***}P < 0.001$, $^{****}P < 0.0001$.

following LPS injury was 5% (data not shown). The change in body weight as the injured mice recovered showed that the mice were recovering by 7 days, when the Tregs were isolated (Figure 2A).

For transcriptome analysis, we employed a statistical methodology based on linear models with empirical Bayes statistics, available from the limma package, to calculate moderated t-statistics and to identify differentially regulated transcripts between Treg sets (23, 24). Such an approach is analogous to shrinking estimated sample variances toward a pooled estimate among multiple genes, which was demonstrated to be more robust and improve inferences at both the gene and gene set levels (23, 25), particularly in small data sets. The array data set expression values are normalized and then analyzed with the limma package as an integrated whole, as previously described (23, 24). We identified 1,599 differentially expressed transcripts between Treg sets using this method when filtering at an adjusted $P <$ 0.05 and a fold change >2 (transcripts listed in Supplemental Tables 1–3).

Principal component analysis (PCA) of gene expression of sorted Tregs between the 3 conditions showed that the top 3 principal components accounted for 52% of the variance in between Treg sets (Figure 2B). The numbers of transcripts that were up- or downregulated for each comparison are shown in Table 1.

A Venn diagram demonstrates overlap of differentially expressed transcripts (Figure 2C and Supplemental Tables 1–3). Tregs from lungs at 7 days after injury differentially expressed 80 transcripts coding for 78 unique genes, when compared with the expression profile of Tregs from control lungs (resolving lung Tregs vs. control lung Tregs) (Figure 2C; transcripts listed in Supplemental Table 1). Tregs from lungs differentially expressed 1,033 transcripts compared with the Tregs from spleens of the same mice at 7 days after injury (resolving lung Tregs vs. resolving splenic Tregs) (Figure 2C; transcripts listed in Supplemental Table 2).

Unsupervised hierarchical clustering of the 1,599 transcripts demonstrated that each experimental array sample clustered first into their respective location (lung compared with spleen) and then by treatment (control lung Tregs compared with resolving lung Tregs) (Figure 2D). The heatmap depicts the

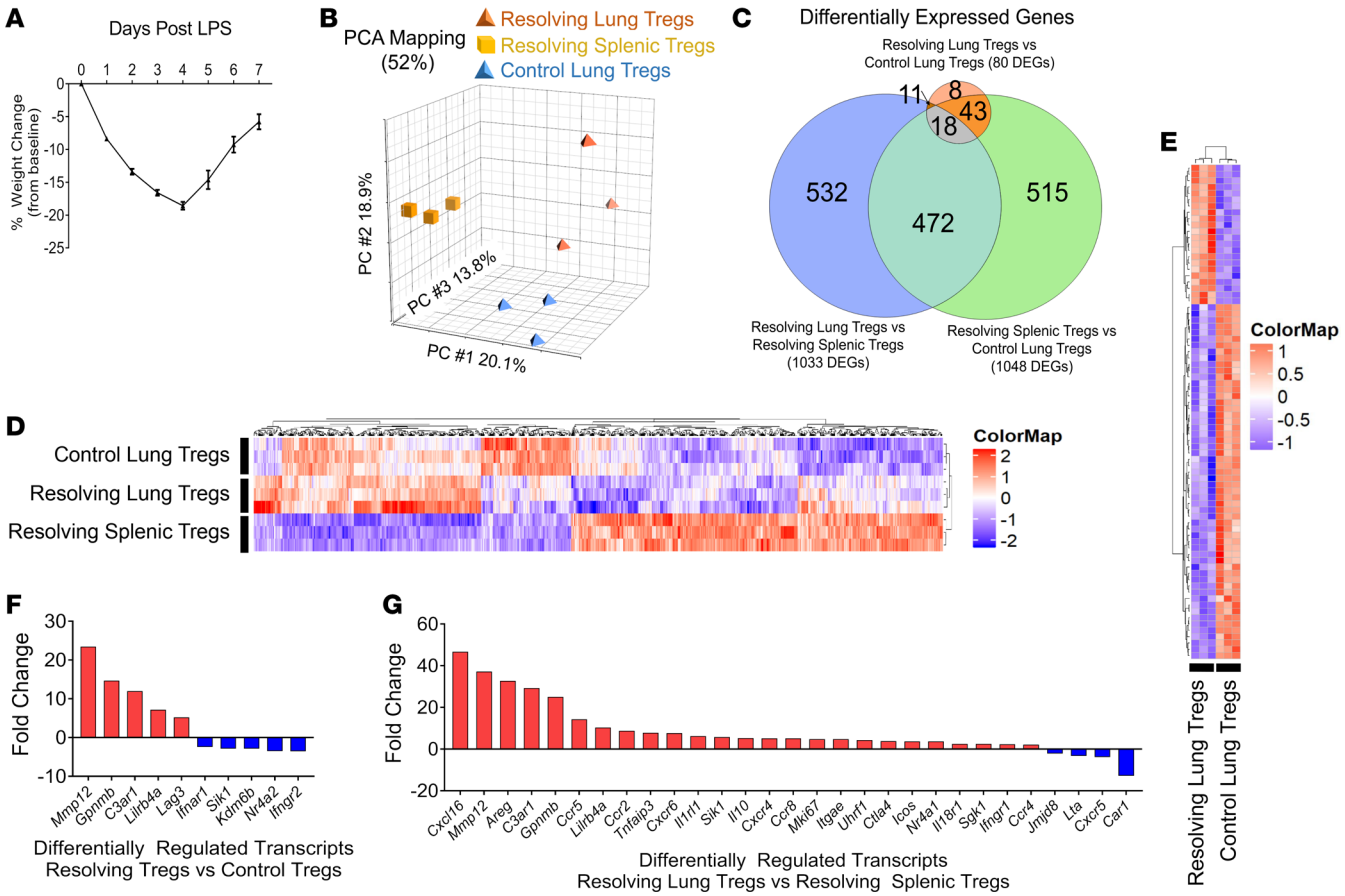

Figure 2. The impact of both an inflammatory stimulus and location on the Treg transcriptome. Tregs were isolated from the lungs of unchallenged *Foxp3*^{EGFP} mice or from the lungs and spleens from *Foxp3*^{EGFP} mice 7 days after LPS (3 mg/kg i.t.) challenge. (**A**) Body weight relative to baseline measured daily before and after injury (n = 19 females; 39 males; 58 total). Data are expressed as the mean ± SEM. (**B**) Principal component analysis (PCA) of mRNA expression demonstrating the contribution of the top 3 principal components to the variance in the 3 Treg sets. Each symbol represents 1 sort of pooled Tregs from mice (15–27 mice/experiment); 3 arrays/set. (**C**) Venn diagram showing the overlap of significantly differentially expressed transcripts between sets (adjusted $P < 0.05$, fold change > 2). Area of the circles reflects the relative number of differentially expressed transcripts for each comparison. Numbers in parentheses indicate the total from the respective pairwise comparison. These transcripts are listed in Supplemental Tables 1–3. (**D**) Unsupervised hierarchical clustering with Euclidean distance metric of 1,599 differentially expressed transcripts identified in all 3 comparisons. The dendrogram identifies clustering across transcripts (top) or across experimental samples (right). The heatmap depicts the $\log_2$ normalized intensity, and each row represents Treg RNA from a pooled set of mice. As described in the Methods, transcripts between sorted Treg sets were identified by filtering at adjusted $P < 0.05$ and fold change > 2 (bright blue for lower expression levels and bright red for high expression levels). (**E**) Differentially expressed genes (DEGs) between resolving lung Tregs and unchallenged lung Tregs. Unsupervised hierarchical clustering of the unique 78 DEGs between lung Treg samples. The heatmap depicts the $\log_2$ normalized intensity across samples. Each column represents Treg RNA from pooled Tregs, and each row represents a DEG. The dendrogram identifies clustering across experimental samples (top) or DEGs (right). (**F**) Select list of transcripts with a >2-fold change between resolving lung Tregs and unchallenged lung Treg comparisons. (**G**) Select list of transcripts with a >2-fold change between resolving lung Tregs and resolving splenic Treg comparisons.

$\log_2$ normalized intensity across samples (bright blue for lower expression levels, and bright red for high expression levels). Each column represents a transcript, and each row represents a replicate of Treg RNA from a pooled set of Tregs.

Unsupervised hierarchical clustering of the 80 differentially expressed transcripts between resolving lung Tregs and control lung Tregs is shown in Figure 2E. The dendrogram identifies clustering across samples (top) or differentially expressed genes (DEGs; left). Twenty-three transcripts were upregulated, including *Mmp12*, *C3ar1*, and *Lag3*. Fifty-seven transcripts were downregulated, including *Sik1* and *Kdm6b*. Interestingly, transcripts such as *C3ar1*, *Kdm6b*, *Mmp12*, and *Sik1*, which have little to no known role in Treg function, also showed significant differential expression between control lung Tregs compared with resolving lung Tregs (Figure 2F).

Transcripts previously demonstrated to be differentially regulated by Tregs during influenza-induced lung injury, such as *Areg*, *Ctla4*, and *Itgae* (CD103) (13), were found to be differentially expressed in our data

Table 1. The number of up- or downregulated transcripts that were significantly differentially expressed between the 3 Treg sets

Comparison of Treg sets	Number of transcripts		
	Upregulated	Downregulated	Total
Resolving lung Tregs vs. control lung Tregs	23	57	80 (5%)
Resolving lung Tregs vs. resolving splenic Tregs	514	519	1033 (65%)
Control lung Tregs vs. resolving splenic Tregs	464	584	1048 (65%)

The transcripts are upregulated or downregulated >2-fold and are filtered at an adjusted $P < 0.05$. Percentage (%) describes the percentage of the total number of transcripts (1,599).

set of transcripts expressed by Tregs when resolving lung Tregs are compared with resolving splenic Tregs (Figure 2G). Interestingly, numerous chemokines, cytokines, and chemokine and cytokine receptors were differentially expressed, including *Ccr2*, *Ccr5*, *Cxcl15*, *Cxcl16*, *Cxcr4*, *Cxcr5*, *IL10*, *Il1rl1*, and *Il18r1* (Figure 2G).

To identify biological pathways that may contribute to Treg-directed lung repair, we performed Gene Set Enrichment Analysis (GSEA) using gene sets derived from the public Gene Ontology (GO) database (http://www.geneontology.org/) and the rotation gene set tests (ROAST) statistical gene set test (26, 27). When the resolving lung Tregs are compared with the control lung Tregs, 13 significant gene sets were identified (Table 2).

Only 1 gene set was enriched and uniquely identified in comparisons of Tregs sorted from resolving lung Tregs and control lung Tregs. This gene set describes an oligosaccharide lipid intermediate biosynthetic process (GO0006490) that results in the formation of an oligosaccharide-lipid intermediate — for example, a molecule of dolichol-phosphate-mannose or dolichol-phosphate-glucose used in posttranslational modification regulating protein folding, trafficking, and degradation (28). This pathway is important in glycosylation of receptors on other lymphocytes, and its role in regulation of receptors on Tregs has not been studied. One gene set was uniquely dampened in Tregs from resolving lung Tregs compared with control lung Tregs. This gene set described genes involved in the positive regulation of glucose metabolic process (GO0010907).

More than 800 gene sets were enriched or dampened in Tregs from resolving lungs compared with spleens. Selected interesting examples of enriched gene sets (Table 3) include tolerance induction (GO0002507), regulation of Treg differentiation (GO0045589), and lymphocyte migration (GO0073676). Dampened gene sets include regulation of notch signaling pathway (GO0008593), T cell receptor signaling pathway (GO0050852), and histone methylation (GO0032481). Taken together, these analyses have identified differentially regulated processes that suggest roles for Tregs in lung repair and that document a tissue-specific expression pattern for Tregs.

Treg CD103$^+$ and IL18$^+$ subsets increase in the lung during resolution of LPS-induced ALI. These results from transcriptional profiling suggested that many potentially novel and exciting changes in Treg function are occurring, which led to studies immunophenotyping Tregs during resolution. First, lymphocyte kinetics in the lung and spleen during resolution were compared with uninjured lungs. The percentage of CD4$^+$ cells increased in the lung during resolution as a proportion of total lymphocytes, whereas in the spleen, the percentage decreased (Figure 3A). The percentage of Foxp3$^+$ cells as a proportion of total CD4$^+$ cells increased significantly in both organs (Figure 3B). The Foxp3$^+$ fluorescence intensity increased significantly in both organs during ALI resolution in the Foxp3$^+$ population (Figure 3C).

Second, transcriptome profiling showed that *Itgae* (CD103), *Il1rl1* (ST2), and *IL18r1* transcripts were upregulated in Tregs from resolving lungs compared with spleen. To investigate if these transcriptional changes correlate with surface expression of these gene products, Foxp3$^+$ cells were examined by flow cytometry for expression of CD103, IL-18 receptor 1 (IL-18R1), and IL1RL1 (ST2). The percentage of Foxp3$^+$ cells expressing CD103 or IL-18R increased at 7 days after LPS only in the lung and not in the spleen (Figure 3, D and E). The percentage change of ST2$^+$Foxp3$^+$ cells between conditions also correlated with the array transcriptional changes. The percentage of total Foxp3$^+$ cells that express ST2$^+$ actually decreased at day 7 after LPS in both the lung and spleen compared with uninjured Tregs in each tissue type (Figure 3F); however, the absolute number of ST2$^+$Foxp3$^+$ cells increased, likely driven by the overall increase in Treg numbers. Most importantly, the total number of lung Tregs expressing these 3 receptors was significantly increased in resolving lungs compared with uninjured lungs (Figure 3, G–I).

Table 2. Comparison: Resolving lung Tregs vs. control lung Tregs

Upregulated in resolving lung Tregs			Downregulated in resolving lung Tregs		
Ontology ID	**Functional term**	**Number of genes**	**Ontology ID**	**Functional term**	**Number of genes**
GO0046500	S-adenosylmethionine metabolic process	10	GO0007176	Regulation of epidermal growth factor-activated receptor activity	14
GO0006490	*Oligosaccharide lipid intermediate biosynthetic process*	11	GO0007175	Negative regulation of epidermal growth factor activated receptor activity	10
GO0006490	Vesicle transport along microtubule	31	GO0061099	Negative regulation of protein tyrosine kinase activity	17
			GO0009712	Catechol-containing compound metabolic process	19
			GO0010907	*Positive regulation of glucose metabolic process*	24
			GO2000272	Negative regulation of receptor activity	17
			GO0006584	Negative regulation of epidermal growth factor receptor signaling pathway	18
			GO0006584	Catecholamine metabolic process	19
			GO0031958	Corticosteroid receptor signaling pathway	13
			GO1901185	Negative regulation of ERBB signaling pathway	19

Gene Set Enrichment Analysis identified Gene Ontology Biological Pathways showing highly significant enrichment between Treg sets. All significant gene sets that were differentially regulated between resolving lung Tregs and control lung Tregs comparisons are listed. The 2 gene sets unique only in this comparison are identified in italics. Sets have a FDR < 0.1.

Given the differential expression of both the IL-18 receptor and IL-33 receptor transcripts in resolving lung Tregs, the expression kinetics of these 2 cytokines was examined. Both IL-18 and IL-33 peaked in concentration in BAL supernatant fluid at day 1 after LPS injury (Supplemental Figure 2, A and B).

Expression of chemokines and cytokines in BAL supernatants during LPS-induced ALI. Based on the differential expression of cytokine and chemokine receptors, we measured the changes in cytokines and chemokines present in the lungs before Tregs increase, testing the hypothesis that early immune signaling drives subsequent Treg recruitment and function during resolution of ALI. The lungs of WT mice given LPS were lavaged at day 1, 3, 7, or 10 after injury and compared with control, uninjured lung BAL fluid. The quantities of 23 cytokines and chemokines were determined (Table 4; graphical representation of several of these cytokines and chemokines are plotted in Supplemental Figure 2, C–G). The gene profiling data demonstrate increased expression of mRNAs for CCR5, CCR2, and CXCR3. CCR5 is the receptor for CCL3 (MIP-1α), as well as for CCL4 (MIP-1β) and CCL5 (RANTES). The concentrations in the BAL supernatant of these 3 chemokines are greatest early in LPS-induced injury, days 1–3 (Table 4 and Supplemental Figure 2, C–E).

The chemokine receptor CCR2 mRNA is significantly increased in resolving lung Tregs when compared with resolving spleen Tregs. Its respective chemokine, CCL2 (MCP-1), peaks in concentration at day 3 following LPS-induced lung injury (Table 4 and Supplemental Figure 2F).

Treg-depleted mice have increased immune cell numbers during ALI lung resolution. To determine the impact Treg depletion has on ALI resolution, we compared resolution in 2 transgenic strains, the *Foxp3*^{EGFP} strain used for the transcriptomic analysis and the *Foxp3*^{DTR} strain, which expresses both the human diphtheria toxin (DT) receptor (DTR) and GFP in the 3′ untranslated region of the Foxp3 locus and allows for depletion of endogenous Tregs when DT is administered (29). By administering DT to the *Foxp3*^{DTR} strain, we can examine the LPS-induced lung injury and recovery in the presence (*Foxp3*^{EGFP}) or absence (*Foxp3*^{DTR}) of Tregs (Figure 4A). Mice depleted of Tregs during ALI have similar weight loss and recovery compared with control at this dose of LPS (Figure 4B); however, Treg-depleted mice have increased cellularity, as demonstrated both by histopathology of lung tissue at 7 days after LPS (Figure 4C) and total number of cells obtained from enzymatic single cell lung suspensions (Figure 4D). Treg depletion was confirmed by decreased CD4$^+$Foxp3$^+$ lymphocytes in the Treg-depleted mice (Figure 4E). Furthermore, Treg-depleted mice had elevated numbers of neutrophils, alveolar macrophages, and interstitial macrophages, as determined by total numbers in single cell suspensions using a published flow cytometric panel and gating

Table 3. Comparison: Resolving lung Tregs vs. resolving splenic Tregs

Upregulated in resolving Lung Tregs			Downregulated in resolving lung Tregs		
Ontology ID	**Functional term**	**Number of genes**	**Ontology ID**	**Functional term**	**Number of genes**
GO0002507	Tolerance induction	23	GO0000959	Mitochondrial RNA metabolic process	28
GO0002028	Regulation of sodium ion transport	44	GO0030488	tRNA methylation	20
GO0045589	Regulation of regulatory T cell differentiation	19	GO0031063	Regulation of histone deacetylation	22
GO0002825	Regulation of T-helper 1 type immune response	20	GO0008593	Regulation of Notch signaling pathway	42
GO0010574	Regulation of vascular endothelial growth factor production	20	GO0038202	TORC1 signaling	20
GO0072676	Lymphocyte migration	57	GO0050852	T cell receptor signaling pathway	65
GO0070849	Response to epidermal growth factor	24	GO0001912	Positive regulation of leukocyte mediated cytotoxicity	34
GO1902622	Regulation of neutrophil migration	28	GO0016571	Histone methylation	108
GO0050715	Positive regulation of cytokine secretion	74	GO0032481	Positive regulation of type I interferon production	37
GO0035794	Positive regulation of mitochondrial membrane permeability	23			
GO0071277	Cellular response to calcium ion	29			

Gene Set Enrichment Analysis identified Gene Ontology Biological Pathways showing highly significant enrichment between Treg sets. Selected gene sets of interest that were differentially regulated between resolving lung Tregs and resolving splenic Tregs comparisons are listed. Sets are listed only if FDR < 0.1.

approach (Figure 4, F–J) (30). We also detected differences in lymphocyte subsets numbers in the single cell suspensions between the 2 conditions. The numbers of $CD3^+$, $CD4^+$, and $CD8^+$ lymphocytes were increased, and $\gamma\delta^+$ T cell and $CD19^+$ lymphocytes were decreased in Treg-depleted mice (Figure 4, K–Q; lymphocyte gating scheme described in Supplemental Figure 3).

Tregs from LPS-treated lungs increase expression of Mmp12. *Mmp12* was one of the most highly expressed DEGs in Tregs during ALI resolution compared with either of the other conditions (Figure 2, F and G). To confirm Treg expression of *Mmp12* transcripts, we sorted Tregs (GFP^+ lymphocytes) from the lungs of *Foxp3*^{EGFP} mice that were either uninjured or 7 days after LPS injury, when the ALI is resolving, to obtain highly purified $Foxp3^+$ cells. Tregs from resolving ALI expressed many fold more *Mmp12* transcripts compared with uninjured Tregs (Figure 5A).

Treg-depleted mice repleted with Tregs lacking MMP12 expression have more lung neutrophils during resolution of LPS-induced ALI. To begin to determine the role of MMP12 expressed by Tregs in mediating inflammation resolution, we performed adoptive transfer experiments of either *Foxp3*^{EGFP} (*Mmp12*$^{+/+}$) or *Mmp12*$^{-/-}$ Tregs into Treg-depleted (*Foxp3*^{DTR}) mice (Figure 5B) (16). The data show that, by day 7 after injury, mice exposed to LPS and repleted with either *Mmp12*$^{+/+}$ or *Mmp12*$^{-/-}$ Tregs have begun to recover from their weight loss due to the injury, which nadirs at day 4 after LPS (Figure 5C). Total BAL cell numbers, BAL total protein concentration, and total lung cell count in the enzymatically digested single cell suspensions at day 7 after injury remain similar between *Mmp12*$^{+/+}$ or *Mmp12*$^{-/-}$ Treg-repleted mice (Figure 5, D–F). The number of $Foxp3^+$ cells in single cell suspensions generated from lung digests following lung lavage was not significantly different between the 2 conditions (Figure 5G). Moreover, we did not detect any differences in lymphocyte subsets in the single cell suspensions between the 2 conditions ($CD3^+$, $CD4^+$, $CD8^+$, $\gamma\delta^+$, NK, and NK T cells; Supplemental Figure 4). Further immunophenotyping of macrophage, monocyte, and neutrophil populations (Figure 5, H–L) using a published flow cytometric panel and gating approach (30) demonstrated that *Foxp3*^{DTR} mice depleted of endogenous Tregs and then repleted with *Mmp12*$^{-/-}$ Tregs at the time of injury had greater numbers of neutrophils and a trend for increased interstitial macrophages compared with *Foxp3*^{DTR} mice repleted with *Mmp12*$^{+/+}$ Tregs (Figure 5, I and J).

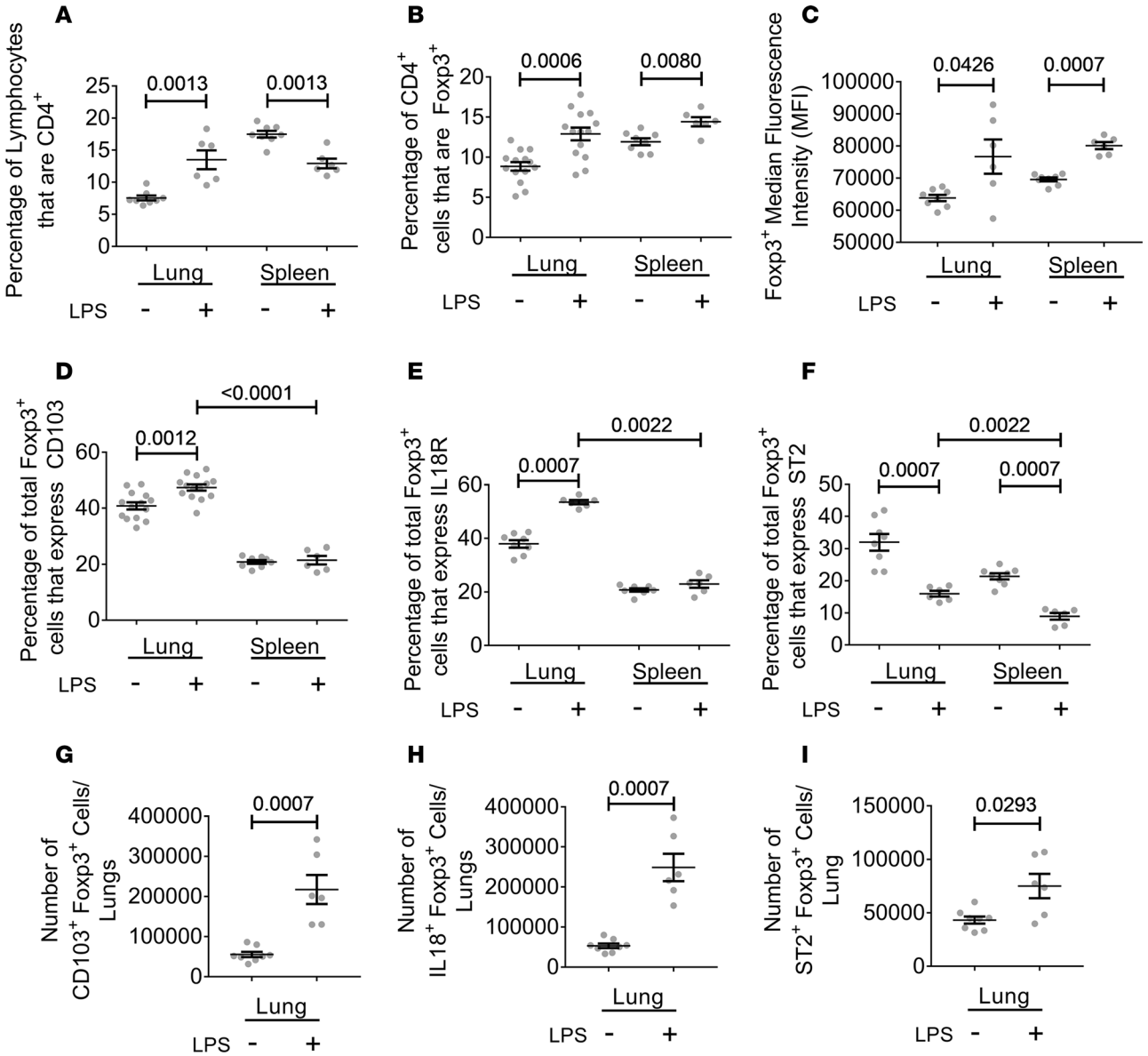

Figure 3. Protein expression of receptors and other surface molecules on Foxp3⁺ Tregs in the lung and spleen and their numbers in lung during ALI resolution compared with unchallenged mice. *Foxp3*^{EGFP} mice were challenged with LPS (3 mg/kg i.t.) and compared with unchallenged *Foxp3*^{EGFP} mice (labeled as "LPS–" mice in figures). (**A**) Percentages of CD4⁺ cells were compared with the total number of lymphocytes in the lymphocyte gate determined by flow cytometry in lung or spleen single cell suspensions of unchallenged (control) mice or at 7 days after LPS (n = 6–8 per condition). (**B**) The percentage of total CD4⁺ cells that expressed Foxp3 was determined (n = 6–14 per set). (**C**) Median fluorescence intensity (MFI) of GFP expression driven by the endogenous *Foxp3* promoter was determined in the lung and spleen in unchallenged mice or at 7 days after LPS (n = 6–8 per condition). (**D–F**) Percentages of CD103⁺Foxp3⁺ cells (**D**), IL18R⁺Foxp3⁺ cells (**E**), and ST2⁺Foxp3⁺ cells (**F**) as a percentage of total Foxp3⁺ cells (n = 6–14 per condition). (**G–I**) Numbers of CD103⁺Foxp3⁺ cells (**G**), IL18R⁺Foxp3⁺ cells (**H**), and ST2⁺Foxp3⁺ cells (**I**) determined in the lung between conditions (n = 6–8 per condition). Data are expressed as the mean ± SEM. Mann Whitney rank sum test determined P values.

These results suggest that Treg-expressed MMP12 plays a role in Treg-promoted resolution of the inflammatory process but is not required for Tregs to traffic to the lung or survive there.

Treg-depleted mice repleted with Tregs lacking SIK1 expression have more Tregs in the lung and an increased Treg expression of CD103 during ALI resolution. Salt inducible kinase 1 (*Sik1*) was one of the significantly downregulated DEGs in resolving lung Tregs during ALI resolution compared with control lung Tregs (Figure 2, F and G). *Sik1* encodes a serine/threonine protein kinase that is a member of the adenosine monophosphate-activated kinase (AMPK) subfamily of kinases. It also contains an ubiquitin-associated (UBA) domain. It is expressed by macrophages and contributes to proinflammatory signaling pathways initiated through TLRs or IL-1 (31, 32). Recently, members of this salt-inducible kinase family have been

Table 4. Cytokines measured in BAL fluid in unchallenged (control) mice or at day 1, 3, 7, or 10 after LPS in WT mice

		Days after LPS			
Analyte (pg/mL)	**Control (*n* = 8)**	**Day 1 (*n* = 11)**	**Day 3 (*n* = 13)**	**Day 7 (*n* = 13)**	**Day 10 (*n* = 11)**
Eotaxin	<LLOQ	574.5 ± 55.8	459.3 ± 29.3	<LLOQ	<LLOQ
G-CSF	4.3 ± 0.8 (*n* = 5) <LLOQ (*n* = 3)	2705601 ± 1940.3	19278.5 ± 2917	87.7 ± 27.1	22.6 ± 12.3 (*n* = 7) <LLOQ (*n* = 4)
GM-CSF	28.41 (*n* =1) <LLOQ (*n* = 7)	125.5 ± 33.2	69.3 ± 8.5 (*n* = 12) <LLOQ (*n* = 1)	<LLOQ	<LLOQ
IFN-γ	2.1 ± 1.8 (*n* = 2) <LLOQ (*n* = 6)	12.2 ± 1.6 (*n* = 8) <LLOQ (*n* = 3)	24.7 ± 3.9 (*n* = 12) <LLOQ (*n* = 1)	<LLOQ	<LLOQ
IL-10	1.1 ± 0.8 (*n* = 2) <LLOQ (*n* = 6)	30.3 ± 7.0	25.4 ± 0.9	0.8 ± 0.1 (*n* = 2) <LLOQ (*n* = 9)	0.3 (*n* = 1) <LLOQ (*n* = 10)
IL-12 (p40)	21.4 ± 4.3	155.0 ± 17.5	19655 ± 226.0	114.6 ± 13.0	92.1 ± 8.4
IL-12 (p70)	9.0 ± 4.0 (*n* = 3) <LLOQ (*n* = 5)	80.6 ± 13.5	239.6 ± 29.1	<LLOQ	<LLOQ
IL-13	26.3 ± 9.8 (*n* = 3) <LLOQ (*n* = 5)	111.6 ± 9.3	115.5 ± 4.4	15.5 ± 2.4 (*n* = 7) <LLOQ (*n* = 6)	9.2 ± 4.7 (*n* = 4) <LLOQ (*n* = 7)
IL-17A	3.16 (*n* = 1) <LLOQ (*n* = 7)	7.1 ± 0.9	58.7 ± 7.2	1.19 ± 0 (*n* = 2) <LLOQ (*n* = 11)	<LLOQ
IL-1a	1.22 (*n* = 1) <LLOQ (*n* = 7)	6.5 ± 0.5	16.4 ± 1.4	<LLOQ	1.97 (*n* = 1) <LLOQ (*n* = 10)
IL-1β	8.0 ± 5.5 (*n* = 3) <LLOQ (*n* = 5)	107 ± 9.9	146 ± 11.2	5.36 ± 3.0 (*n* = 2) <LLOQ (*n* = 11)	<LLOQ
IL-2	<LLOQ	<LLOQ	<LLOQ	<LLOQ	<LLOQ
IL-3	0.11 (*n* = 1) <LLOQ (*n* = 7)	2.5 ± 0.3 (*n* = 10) <LLOQ (*n* = 1)	2.2 ± 0.3 (*n* = 12) <LLOQ (*n* = 1)	<LLOQ	<LLOQ
IL-4	<LLOQ	5.6 ± 0.7 (*n* = 10) <LLOQ (*n* = 1)	5.1 ± 0.4 (*n* = 10) <LLOQ (*n* = 3)	<LLOQ	<LLOQ
IL-5	<LLOQ	20.6 ± 3.1	12.6 ± 1.2	2.5 (*n* = 1) <LLOQ (*n* = 12)	<LLOQ
IL-6	<LLOQ	854.4 ± 144.6	2142.3 ± 228.6	10.7 ± 8.3 (*n* = 3) <LLOQ (*n* = 10)	4.0 ± 2.7 (*n* = 2) <LLOQ (*n* = 9)
IL-9	78.4 ± 3.1 (*n* = 3) <LLOQ (*n* = 5)	85.8 ± 4.4 (*n* = 8) <LLOQ (*n* = 3)	<LLOQ	35.8 ± 7.0 (*n* = 3) <LLOQ (*n* = 10)	28.4 ± 4.3 (*n* = 6) <LLOQ (*n* = 5)
KC	5.0 ± 0.8	1389.4 ± 592.7	413.1 ± 62.1	19.5 ± 2.5	4.9 ± 0.8
MCP-1	21.7 ± 8.6 (*n* = 4) <LLOQ (*n* = 4)	747.9 ± 153.8	2517.2 ± 593.3	24.2 ± 4.4 (*n* = 12) <LLOQ (*n* = 1)	10.5 ± 3.0 (*n* = 5) <LLOQ (*n* = 6)
MIP-1α	<LLOQ	1353.8 ± 444.1	799.4 ± 83.4	5.0 ± 1.2	4.1 ± 2.0 (*n* = 3) <LLOQ (*n* = 8)
MIP-1β	0.986 (*n* = 1) <LLOQ (*n* = 7)	837.1 ± 481.4	957.4 ± 129.6	7.0 ± 3.3 (*n* = 6) <LLOQ (*n* = 7)	3.2 (*n* = 1) <LLOQ (*n* = 10)
RANTES	1.17 (*n* = 1) <LLOQ (*n* = 7)	772.0 ± 100.6	829.0 ± 83.5	6.4 ± 1.4	2.4 ± 1.3 (*n* = 4) <LLOQ (*n* = 7)
TNF-α	1.99 (*n* = 1) <LLOQ (*n* = 7)	1192.7 ± 287.2	251.3 ± 50.3	<LLOQ	<LLOQ

Values are mean ± SEM. Samples with values below the lower limit of quantitation (LLOQ) for the assay are noted in the table and not included in the calculation of mean and SEM. The number of samples in each condition (*n*) is shown in the column subheadings unless otherwise indicated in the individual cells. Samples are combined from 2 independent experiments.

demonstrated to play a role in Treg energy homeostasis as one of several important effectors of liver kinase B1 (LKB1) signaling (33).

To examine the role of SIK1 expressed by Tregs in mediating inflammation resolution, we performed adoptive transfer experiments of either *Foxp3*^{EGFP} (*Sik1*$^{+/+}$) or *Sik1*$^{-/-}$ Tregs into Treg-depleted (*Foxp3*^{DTR}) mice (16). The data demonstrate that, by day 7 after injury, mice repleted with either *Sik1*$^{+/+}$ or *Sik1*$^{-/-}$ Tregs have similar weight recovery and total lung cell numbers (Figure 6, A and B). Interestingly, Treg-depleted mice repleted with *Sik1*$^{-/-}$ Tregs have increased Treg numbers in the lung at 7 days after injury and an increased percentage and number of Tregs expressing CD103 during lung resolution, compared with mice repleted with *Sik1*$^{+/+}$ Tregs (Figure 6, C–G). Also, Treg-depleted

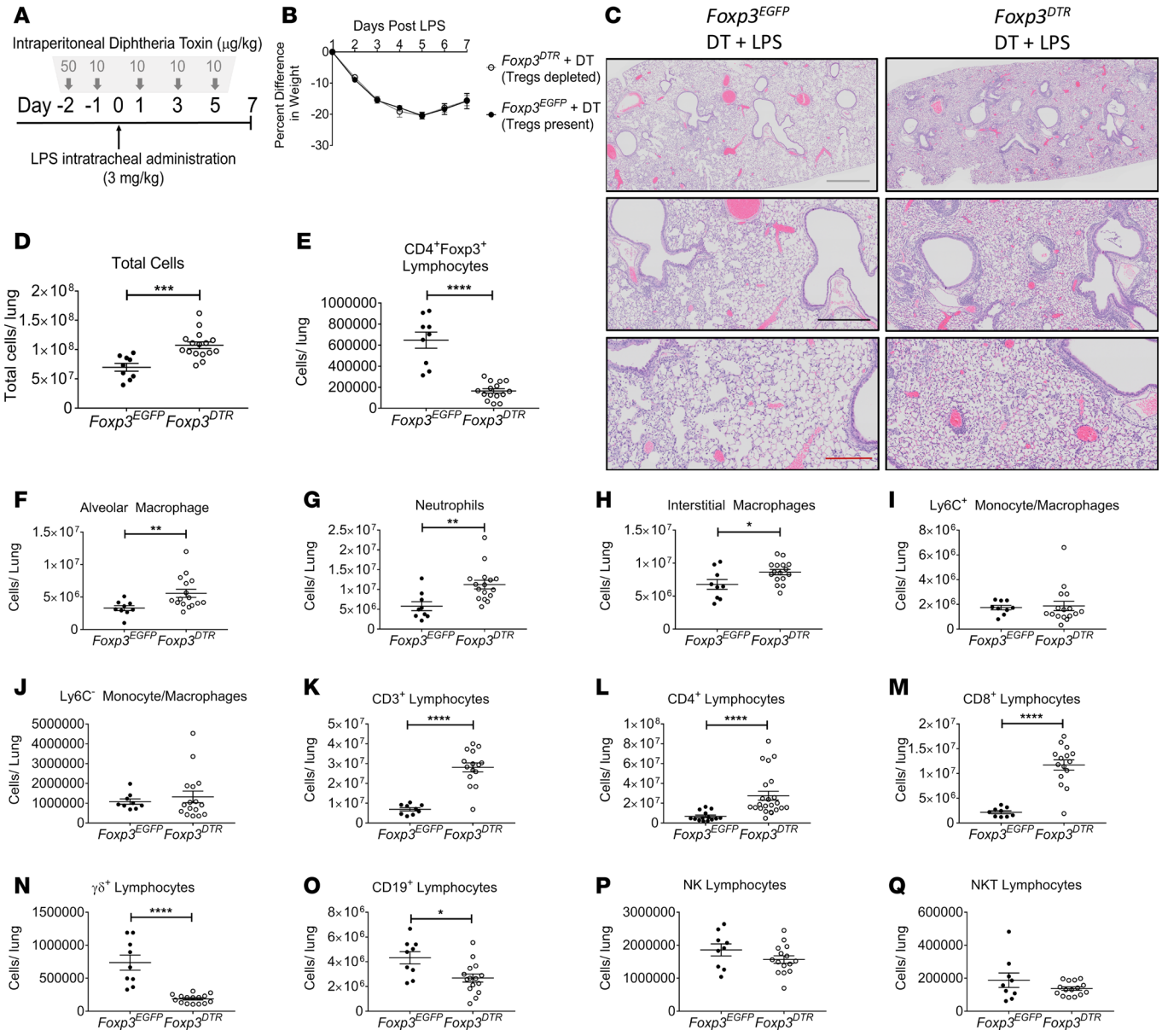

Figure 4. Treg-depleted mice have increased immune cell numbers during resolution of acute lung injury. (**A**) *Foxp3*^{EGFP} or *Foxp3*^{DTR} mice (n = 9–15 per group, combined from 2 separate experiments) were challenged with intraperitoneal diphtheria toxin (DT; 50 μg/kg or 10 μg/kg) administered at days –2, –1, 1, 3, and 5 along with intratracheal LPS was administered at day 0. Mice were examined at 7 days after LPS for immune cell populations. (**B**) Body weight relative to baseline determined after injury. (**C**) Representative H&E lung sections reveal increased cellularity 7 days after LPS and DT in Treg-depleted mice. Gray scale bar: 1 mM. Black scale bar: 500 μM. Maroon scale bar: 250 μM. (**D**) Total lung cell count from single cell lung suspension obtained at day 7 after DT and LPS treatment demonstrated increase cellularity in Treg-depleted mice. (**E**) Total CD4$^+$Foxp3$^+$ lymphocyte numbers determined and which confirm Treg depletion. (**F–J**) Changes in myeloid cell subsets as total numbers in single cell suspensions determined using a published flow cytometric panel and gating approach (30). Treg-depleted mice had significant increases in alveolar macrophages, neutrophils, and interstitial macrophages. (**K–Q**) Changes in lymphocyte subsets as a total numbers in single cell suspensions determined and demonstrated increased numbers of CD3$^+$, CD4$^+$, and CD8$^+$, γδ$^+$, NK, and NKT lymphocytes. (**N–O**) Numbers of CD19$^+$ and γδ$^+$ lymphocytes were also found at lower numbers in Treg-depleted mice. Data are expressed as the mean ± SEM. P values calculated by Mann Whitney rank sum test. *P < 0.05, **P < 0.01 ***P < 0.001, ****P < 0.0001.

mice repleted with *Sik1*$^{-/-}$ Tregs have decreased Foxp3$^+$ expression, as measured by median fluorescence intensity (MFI) in Foxp3$^+$ cells (Figure 6D). Furthermore, the percentage of Foxp3$^+$ cells that coexpressed IL-18R was increased in *Foxp3*^{DTR} mice repleted with *Sik1*$^{-/-}$ Tregs compared with *Sik1*$^{+/+}$ Tregs (Figure 6H). Studies quantifying myeloid cell subsets demonstrated that *Foxp3*^{DTR} mice depleted of endogenous Tregs and then repleted with *Sik1*$^{-/-}$ Tregs at the time of injury had fewer Ly6C$^-$ monocyte/macrophages compared with *Foxp3*^{DTR} mice repleted with *Sik1*$^{+/+}$ Tregs (Figure 6, I–M). We did

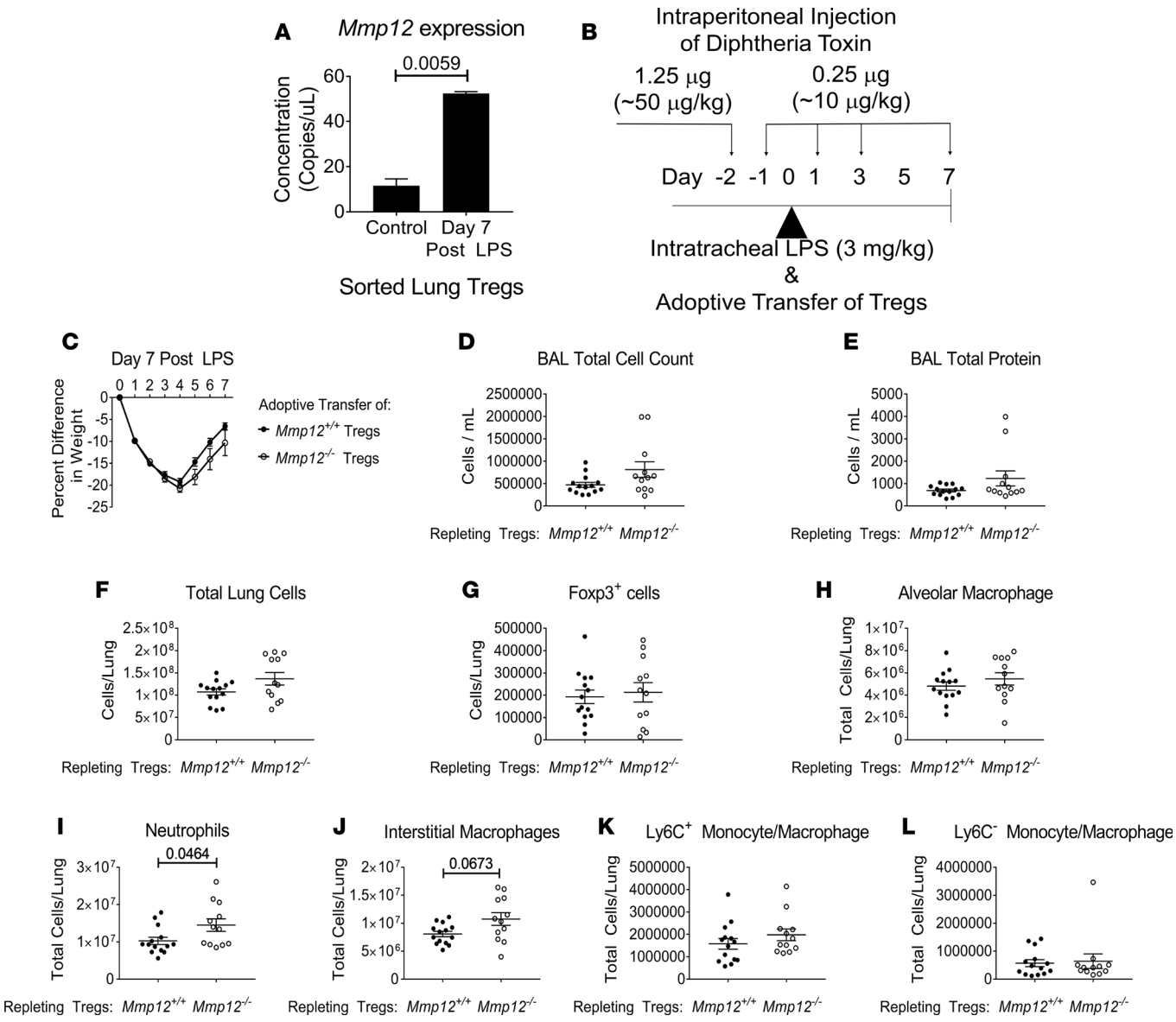

Figure 5. Treg-depleted mice repleted with Tregs lacking MMP12 expression have more neutrophils during lung resolution. (**A**) *Mmp12* transcript concentrations determined by digital droplet RT-PCR analysis. $CD4^+GFP^+$ cells (Tregs) sorted from the lungs of $Foxp3^{EGFP}$ mice either from control lungs or lungs resolving from ALI (n = 2 per group, representative of 3 separate experiments). P value by 2-tailed Student t test. (**B–L**) $Foxp3^{DTR}$ (DTR) mice were given diphtheria toxin (DT) to deplete endogenous Tregs as previously described (16), followed by LPS. One hour after LPS challenge, the DTR mice received 1×10^6 $CD4^+CD25^+$ cells (Tregs) from either $Foxp3^{EGFP}$ or $Mmp12^{-/-}$ mice. n = 12–14 per group, combined from 2 separate experiments. Samples are combined from 2 independent experiments (**B**). Adoptive transfer of $Mmp12^{-/-}$ Tregs have similar weight recovery (**C**), BAL cell counts (**D**), and BAL total protein (**E**) after LPS-induced ALI compared with $Foxp3^{EGFP}$ Tregs ($Mmp12^{+/+}$) 7 days after LPS administration. Total lung cell count and the number of Tregs between the adoptive transfer conditions did not differ (**F** and **G**). Changes in myeloid cell subsets as total numbers in single cell suspensions determined using a published flow cytometric panel and gating approach (30) (**H–L**). $Foxp3^{DTR}$ mice depleted of endogenous Tregs and then repleted with $Mmp12^{-/-}$ Tregs at the time of injury had greater neutrophil cell numbers and a trend for increased interstitial macrophages numbers compared with $Foxp3^{DTR}$ mice repleted with $Mmp12^{+/+}$ Tregs 7 days after LPS administration (**I–J**). Data are expressed as the mean ± SEM. P values calculated by Mann Whitney rank sum test.

not detect any differences in lymphocyte subsets between the 2 conditions ($CD3^+$, $CD4^+$, $CD8^+$, $\gamma\delta^+$, NK, and NK T cell numbers; Supplemental Figure 5).

Discussion

In this report, we explored the global transcriptional changes occurring in Tregs during resolution of lung injury. We compared uninjured lung Treg expression profiles with lung Tregs isolated 7 days after injury, as earlier studies demonstrated that $Foxp3^+$ Treg numbers peak at this time point and directly enhance alveolar

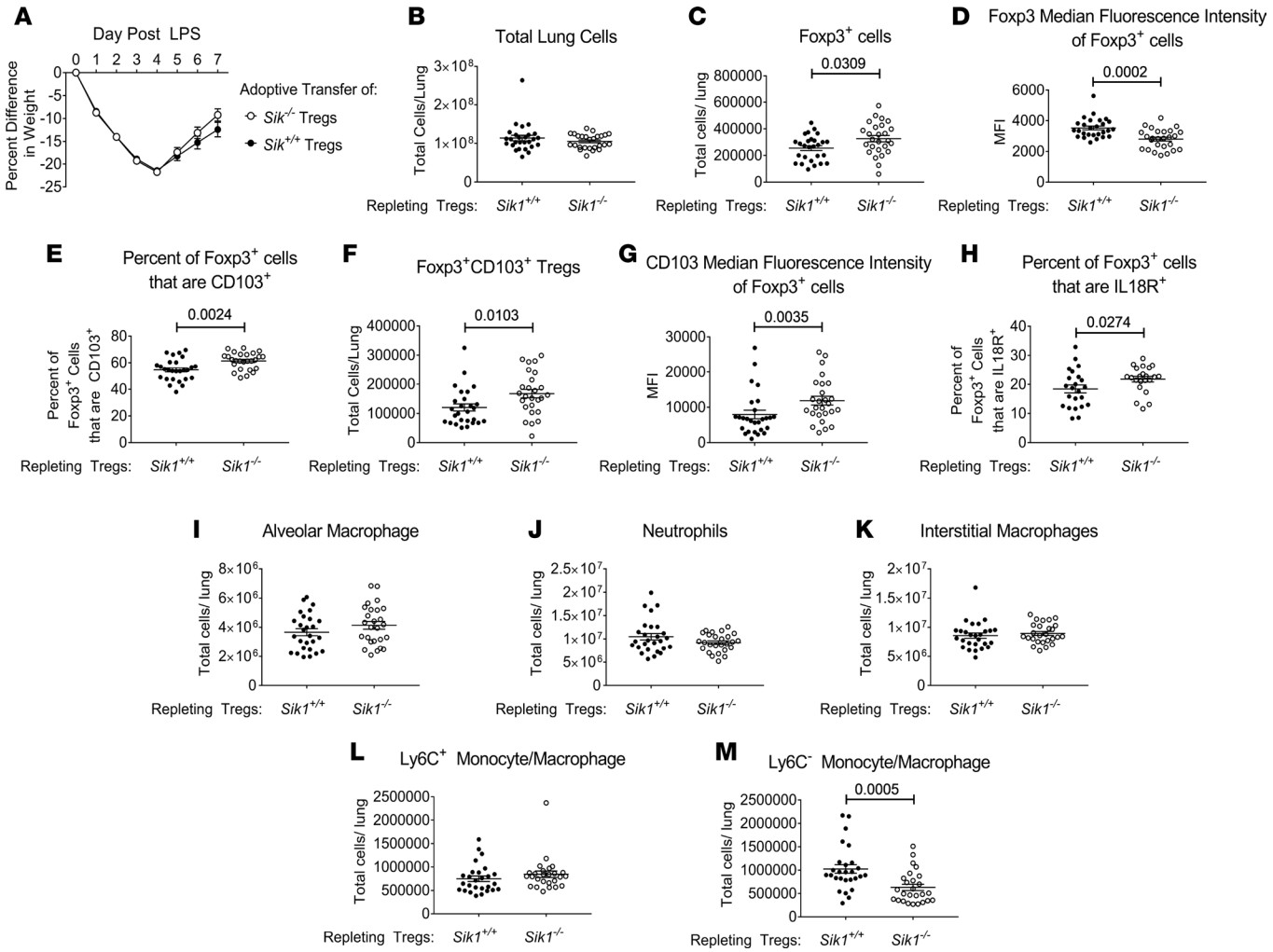

Figure 6. Treg-depleted mice repleted with Tregs lacking SIK1 expression have more Tregs and increased Treg CD103 expression during lung resolution. *Foxp3*^{DTR} (DTR) mice were given diphtheria toxin (DT) to deplete endogenous Tregs as previously described (16), followed by LPS. One hour after LPS challenge, the DTR mice received 1 × 10^6 CD4$^+$CD25$^+$ cells (Tregs) from either *Foxp3*^{EGFP} or *Sik1*$^{-/-}$ mice. Samples are combined from 4 independent experiments (n = 22–35 per group). (**A**) Weight recovery after LPS-induced ALI is similar after adoptive transfer of *Sik1*$^{-/-}$ Tregs compared with *Foxp3*^{EGFP} Tregs (*Sik1*$^{+/+}$) 7 days after LPS administration. (**B**) Total lung cell count did not differ between the adoptive transfer conditions. (**C–E**) *Foxp3*^{DTR} mice depleted of endogenous Tregs and then repleted with *Sik1*$^{-/-}$ Tregs at the time of injury had greater numbers of Foxp3$^+$ cells (**C**), decreased Foxp3$^+$ expression as measured by median fluorescence intensity (MFI) in Foxp3$^+$ cells (**D**), and a greater percentage of Foxp3$^+$ cells coexpressing CD103 (**E**). (**F–G**) The increased percentage of Foxp3$^+$ cells expressing CD103$^+$ correlated with a greater number of Foxp3$^+$CD103$^+$ Tregs (**F**) and a higher expression of CD103 in Tregs as measured by MFI (**G**). (**H**) The percentage of Foxp3$^+$ cell that coexpressed IL18R was also increased in *Foxp3*^{DTR} mice repleted with *Sik1*$^{-/-}$ Tregs compared with *Sik1*$^{+/+}$ Tregs. (**I–M**) Changes in myeloid cell subsets as total numbers in single cell suspensions determined using a published flow cytometric panel and gating approach (30). *Foxp3*^{DTR} mice depleted of endogenous Tregs and then repleted with *Sik1*$^{-/-}$ Tregs at the time of injury had less Ly6C$^-$ monocyte/macrophage numbers compared with *Foxp3*^{DTR} mice repleted with *Sik1*$^{+/+}$ Tregs. Data are expressed as the mean ± SEM. *P* values calculated by Mann Whitney rank sum test.

epithelial proliferation in 2 mouse models of lung regeneration (11). Tregs increased 3.7-fold in the *Foxp3*^{EGFP} mice, which is a similar change compared with other reports (11). Our studies demonstrate how Tregs regulate their transcriptional profile during ALI and that Tregs display heterogeneity in their responses, likely reflecting variation in the microenvironment. This heterogeneity may suggest functional variations within the Treg population important for spatial variation in the process of resolution within the distal lung. Furthermore, there are tissue-specific transcriptional differences during injury, which also show heterogeneity.

Tregs function in 2 major ways; they serve to modulate immunosuppression, and they participate in the resolution and repair of damaged tissue. Some of the immunosuppressive effects occur through Treg-expressed molecules, such as CD39, CD73, CTLA-4, galectin, glucocorticoid-induced TNFR-related protein (GITR), granzyme-B, IL-10, IL-35, lymphocyte-activation gene 3 (LAG-3), neuropilin, perforin, and TGF-β (34–36).

Effector CD44^{hi} Tregs have been previously demonstrated to upregulate many of the above factors (35), and *Cd44* mRNA expression is 2.4-fold greater in lung Tregs compared with spleen Tregs during LPS injury in our studies (Supplemental Table 2). However, many of these molecules are not changed in Tregs from injured compared with uninjured lungs at 7 days, suggesting that, at this time point of ALI resolution, Tregs are not transcriptionally regulating these factors, such as *Entpd*1 (CD39), *Gzmb*, and *Il10*.

Beyond their immunosuppressive roles, Tregs function in tissue repair through the expression of growth factors, including AREG and KGF (13, 14, 16). Our data demonstrate that, during the reparative process, Tregs from resolving lungs increase their expression of *Areg* compared with unchallenged lung Tregs and with resolving splenic Tregs.

Our transcriptome data place resolving lung Tregs in more activated states compared with splenic Tregs obtained from the same mice. A recent study using single cell RNA sequencing (scRNAseq) demonstrated heterogeneity in unstimulated Tregs from murine spleens and suggested that Treg subpopulations can be defined based on temporal changes in activation state (37). Our data show that resolving lung Tregs express increased *Nr4a1* mRNA, which is an orphan nuclear receptor that increases early in TCR-mediated activation (37). Moreover, increased expression of *Ccr2*, *Cxcr3*, and *Itgae* are also associated with strongly activated Treg phenotypes (37). *Il18r1* and *Il1rl1*, the receptors for the cytokines IL-18 and IL-33, are transcriptionally upregulated in lung Tregs compared with splenic Tregs from mice with resolving ALI (Figure 2G). The increases in surface expression of CD103 (*Itgae*) and IL-18R in lung Tregs during ALI resolution determined by immunophenotyping show that these genes are translated and may be functionally important (Figure 3, D–E). While the percentage of Tregs that express CD103 increases approximately 25%, this correlates with a 3.9-fold increase in the number of lung CD103$^+$ Tregs. Our prior work demonstrates that blocking CD103 interaction with its receptor, E-cadherin, results in fewer Tregs retained in the lung after LPS-induced ALI and abrogates Treg-promoted epithelial repair (11). The increased size of the Treg population that expresses either CD103, ST2, or IL-18R suggests that subpopulations develop, which are likely to have functional importance during resolution of ALI (37, 38).

Tregs differentially express several chemokine receptors during ALI resolution, including upregulation of CCR2, CCR5, and CXCR4 and downregulation of CXCR5 (Figure 2G). The CCR2 ligand CCL2 (MCP-1) peaks in concentration within the alveolar space at day 3 (Table 4 and Supplemental Figure 2F). The expression of 3 CCR5 receptor ligands, — CCL3 (macrophage inflammatory protein-1a, MIP-1α), CCL4 (MIP-1β), and CCL5 (RANTES) — peaks from days 1–3 (Table 4 and Supplemental Figure 2, C–E). The ligand for the CXCR4 receptor is CXCL12 (stromal cell–derived factor 1; SDF-1). CXCL12 has been shown to be important for repair of the alveolar epithelium after ALI (39). How these chemokines modulate Treg recruitment and retention, as well as the Treg-mediated repair of the alveolar septa, is left to be determined.

Interestingly, differential expression of other gene transcripts, including *Sgk1* and *Mmp12*, were found in resolving lung Tregs compared with resolving splenic Tregs (Figure 2G). Prior work has demonstrated that the serum/glucocorticoid-regulated kinase, SGK1, mediates increased IFN-γ expression by Tregs and results in defects in Treg function (19). *Sgk1* expression increases 2.5-fold in resolving lung Tregs compared with resolving splenic Tregs (Figure 2G and Supplemental Table 2). Based on prior work, this increase may suggest a shift toward a Th1-proinflammatory Treg phenotype, as marked by an increase in CXCR3 (19), which is also increased in resolving lung Tregs compared with resolving splenic Tregs (Supplemental Table 2). These data suggest that Tregs show heterogeneity at this time point. Our studies suggest that understanding Treg plasticity during ALI resolution will be fruitful.

To our knowledge, expression of metalloproteinases (MMPs) such as MMP12 by Tregs has not been identified in lung Tregs; however, the role for MMPs in tissue repair and ALI has been an area of much investigation (40). *Mmp12* expression increases 23-fold in resolving lung Tregs compared with control lung Tregs and 37-fold in resolving lung Tregs compared with resolving splenic Tregs (Figure 2, F and G, and Supplemental Tables 1 and 2). To further pursue the functionalities of Treg-specific expression of MMP12 in ALI resolution, we carried out adoptive transfer of *Mmp12*$^{+/+}$ (*Foxp3*^{EGFP}) and *Mmp12*$^{-/-}$ Tregs. Our data demonstrate that repleting with *Mmp12*$^{-/-}$ Tregs results in more neutrophils in the lung after LPS-induced injury than repleting with *Mmp12*$^{+/+}$ Tregs (Figure 5I), suggesting that Treg-generated MMP12 is important in the resolution of lung injury. The potential role of Treg-expressed MMPs in regulating the processing of chemotactic signals or turnover of the extracellular matrix to promote ALI resolution is unknown. Interestingly, MMP12 plays a role in regulating antiviral immunity by binding to

the promoter of the transcription factor *NFKBIA*, which mediates IFN-α secretion, along with degrading extracellular IFN-α and resolving inflammation (41, 42). Other work has demonstrated that MMP12 cleaves IFN-γ at the c-terminus, which can abrogate IFN-γ signaling (43). Our results propose multiple potential functions and testable hypotheses for Treg-expressed MMP12 in lung repair.

The molecular network that directs Treg functions requires epigenetic programming (44); for example, inhibitors of DNA methyltransferases accelerate resolution of lung inflammation (45). Our studies identified 3 genes, *Uhrf1, Kdm6b,* and *Sik1*, which have well-recognized roles in epigenetic modifications. *Uhrf1* is an ubiquitin ligase (46), and its expression increased 4.31-fold in lung Tregs compared with splenic Tregs during LPS injury in our studies (Figure 2G and Supplemental Table 2). UHRF1 recruits the methyltransferase, DNMT1, to regulate gene expression by modifying chromatin structure (46). Mice with $CD4^+$ T cell–specific deficiency in *Uhrf1* had defective proliferation and functional maturation of colonic Tregs (47). *Kdm6b* (also called *Jmjd3*) codes for another epigenetic modifying factor, a lysine-specific demethylase, that was downregulated 2.89-fold in Tregs after LPS injury (Supplemental Table 1). Previous studies demonstrate that KDM6B is an epigenetic factor in T cell differentiation (48, 49). Ablation of *Kdm6b* affects $CD4^+$ T cell differentiation, and in vitro induction of Tregs was markedly reduced in *Kdm6b*-deficient T cells compared with WT T lymphocytes (48). *Sik1* expression decreased 2.88-fold in resolving lung Tregs compared with control lung Tregs (Figure 2F and Supplemental Table 1). SIK1 is a Ser/Thr kinase that phosphorylates and regulates class II histone deacetylase (HDAC) kinases, among other targets (50). Recently, SIK kinases have been demonstrated to play a role in Treg energy homeostasis as one of several important effectors of LKB1 signaling (33). The role of Treg-expressed SIK1 in lung resolution has not been reported, and our data demonstrate that SIK1 functions in Tregs to regulate CD103 and IL-18 receptor expression, which may help function in retaining Tregs to sites of inflammation and directing Treg immune and metabolic function (33). Thus, our gene expression data support a role for the epigenetic regulation of Treg responses in ALI resolution. Further work investigating epigenetics through multi-omics approaches identifying DNA methylation sites and utilizing chromatin accessibility assays will help further define tissue-specific Treg responses (51).

One limitation of this study is that the adoptive transfer experiments do not fully reconstitute Tregs back to WT numbers, which we have previously reported (11). This may contribute to the modest differences seen in the adoptive transfer experiments and may limit detection of other differences. Future efforts utilizing conditional and cell-specific KOs will more definitively answer these questions, as these tools become available.

Although the Tregs were sorted to high-percent purity, the array data suggest some impurity from sources other than Tregs. For example, surfactant protein transcripts are differentially expressed and upregulated in lung Tregs vs. splenic Tregs. Immunoglobulin transcripts and hemoglobin α and β transcripts are enriched in splenic Tregs. These findings may be due to extracellular vesicles, which can package DNA and mRNAs from other cell types within these organs (52). These vesicles potentially adhere to the Tregs and may, thus, be sorted with them.

Our study did not differentiate the percentage of thymically derived vs. peripherally derived, inducible $Foxp3^+$ Tregs. The distinction and functions of thymically derived $Foxp3^+$ Tregs (tTregs) and $CD4^+$-derived, peripherally induced $Foxp3^+$ Tregs (pTregs) are an active area of investigation (53), and distinguishing between these 2 populations could not be incorporated into our study design. Moreover, the proportion of lung Tregs that are resident lung Tregs and undergo proliferation during ALI resolution vs. the proportion that are circulating and recruited are important questions that remain to be answered. Interestingly, in the 2 resolving Treg populations, the transcript for *Mki67* is upregulated 28-fold in resolving lung Tregs compared with resolving splenic Tregs, suggesting — along with previous work — that Treg proliferation is an important component of the reparative response (12).

In summary, resolution of lung injury is an active process, and understanding the role of the cell types and their interactions in the reparative process is critical for the intelligent development of therapeutic interventions. Our studies identify potential mechanisms of Treg function, both in suppressing the inflammatory response and their recently described tissue-reparative functions. These studies provide insight into transcriptional differences by which Tregs may direct their suppressive or tissue-reparative effects during resolution of ALI and further support the emerging role of Tregs in resolution and repair of lung injury. Understanding prorepair and immune regulatory functions of Tregs and the translation of this work to human diseases such as ARDS may inform studies of Tregs as a cell-based therapy (51, 54, 55).

Methods

Mice. *Foxp3*^{DTR}, *Foxp3*^{EGFP}, and *Mmp12*$^{-/-}$ mice were obtained from the Jackson Laboratory, and colonies of these mice were maintained at the UNC (22, 29, 56). *C57BL/6N-Sik1*$^{tm1.1(KOMP)Vlcg}$ (RRID:MMRRC_049654-UCD) mice were created and archived by Charles River Laboratory from ES cell clone 14108A-D8, generated by Regeneron Pharmaceuticals Inc. and provided to the KOMP Repository (www.komp.org) as part of the KOMP2 Project by Charles River Laboratory (57). Cryopreserved sperm were obtained from KOMP at the UCD (Davis, California, USA). Sperm cryorecovery using C57BL/6J female oocyte donors was performed by the Mutant Mouse Resource and Research Center at UNC through the UNC Cryogenics Core. Mice were bred and housed in ventilated cages within a specific pathogen-free facility at the UNC at Chapel Hill.

Preparation of mice for LPS administration. Eight- to 12-week-old male and female mice were anesthetized with tribromoethanol before tracheal intubation and administration of lipopolysaccharide, *E. coli* LPS O55:B5 (3 mg/kg) (MilliporeSigma), as previously described (11, 12, 16). Mice were studied after 1, 3, 7, or 10 days and were compared with unchallenged age- and sex-matched mice of the same genotype. At endpoints, mice were euthanized by isoflurane overdose and exsanguinated from their inferior vena cava, as previously described (16). Lungs and spleens were removed, and single cell suspensions were generated for flow cytometry analysis or cell sorting, as previously described (11, 16).

DT administration. DT (List Biologicals Laboratories) was suspended in PBS. Stock solutions were thawed once, and mice were injected i.p. with DT as previously described (11, 29).

Isolation of Foxp3^{EGFP} *and Mmp12*$^{-/-}$ *CD4*$^{+}$*CD25*$^{+}$ *Tregs and adoptive transfer*. Spleens from male and female *Foxp3*^{EGFP}, *Mmp12*$^{-/-}$, or *Sik1*$^{-/-}$ mice were removed, and single cell suspensions were prepared. Tregs were then isolated using the EasySep Mouse CD4^{+}CD25^{+} Regulatory T Cell Isolation Kit II per the vendor's protocol (Stemcell Technologies) (16). Adoptive transfer of Tregs (1×10^6) was performed following LPS administration by retro-orbital injection into Treg-depleted *Foxp3*^{DTR} mice as previously reported (16).

Quantifying cytokine and chemokine patterns of alveolar injury in BAL fluid. BAL was performed in unchallenged lungs or at day 1, 3, 7, or 10 after LPS-induced lung injury, as previously described (11, 12). The BAL fluid was centrifuged at 400 *g* to sediment cells, and the supernatants were centrifuged at 1,300 *g* to remove cell debris and other particulates. The Bio-Plex MAGPIX platform (Bio-Rad) was used to measure the levels of 23 cytokines/chemokines in the BAL fluid supernatants per the manufacturer's protocol.

Preparation of lung single cell suspensions for flow cytometry analysis and cell sorting. Lungs were digested by i.t. instillation via a 20-gauge catheter of 1 ml of 5 mg/ml collagenase I (Worthington Biochemical Corp.) and 0.25 mg/mL DNase I (MilliporeSigma) prepared in RPMI media (Invitrogen) prior to instilling 0.5 ml of 1% (wt/vol) low-melting agarose (Invitrogen) similar to previous protocols (16). Lungs were incubated at 37°C for 30 minutes and then minced and triturated through an 18-gauge needle. Cell suspensions were then filtered through a 100-μM filter prior to RBC lysis and stained as previously described (11). For cell sorting experiments, single cell lung digests from 15–27 *Foxp3*^{EGFP} mice were pooled prior to sorting to obtain sufficient Treg numbers and RNA for analysis. For multicolor flow cytometry analysis of lung cells, studies were performed using digests from individual mice.

Multicolor flow cytometry for cell analysis. Single cell suspensions were suspended in buffer (PBS with 1.6 % BSA, MilliporeSigma), and the total cell count was determined by hemocytometer. Cells (1.5×10^6 cells) first underwent Fc receptor blockade using rat anti–mouse FcγRIII/II receptor (CD16/32; BD Biosciences). After blocking for 5 minutes on ice, cells were surface stained using antibodies obtained from BioLegend, eBioscience, or BD Biosciences (Supplemental Table 4). The cells underwent fixation and permeabilization with the Foxp3/Transcription Factor Staining Buffer Set (eBioscience) prior to intracellular staining. A subset of fixed and permeabilized single cell suspensions were stimulated for 3 hours with Cell Activation Cocktail containing phorbol-12-myristate 13-acetate (40.5 μM), ionomycin (660.3 μM), and Brefeldin A (2.5 mg/ml) in DMSO (all from BioLegend). Stimulated cells subsequently stained for lymphocyte populations and identification of specific lymphocytes expressing AREG or KGF determined by flow cytometry using Biotin conjugated anti–mouse Kgf (Biorbyt) and PE conjugated anti-mouse AREG (Biorbyt). Supplemental Table 4 lists antibody clones and catalog numbers for reference. Flow cytometry was performed using a Cytoflex flow cytometer (Beckman Coulter) and analyzed using CytExpert (Beckman Coulter) software.

Multicolor flow cytometric cell sorting. For Treg sorting, single cell digests from *Foxp3*^{EGFP} mice were suspended in buffer (PBS with 1.6 % BSA; MilliporeSigma) containing 33% Percoll (MilliporeSigma). The cell suspension was then centrifuged (931 *g*, 4°C, 20 minutes with low acceleration and deceleration), and the cell pellet containing lymphocytes was suspended in PBS with 1.6% BSA buffer. The lymphocyte suspension was then Fc receptor blocked with rat anti–mouse FcγRIII/II receptor (CD16/32; BD Pharmingen) and surface stained with Alexa 700 conjugated anti–mouse CD4 (Supplemental Table 4). Cells were gated and sorted for CD4$^+$GFP$^+$ cells (Tregs) using a FACSAria instrument and FASCDiva software (Becton Dickinson), and they were analyzed using Flowjo (Tree Star Inc.) software. After sorting, Tregs were flash frozen in liquid nitrogen and later used for RNA purification and analysis.

RNA isolation and analysis. RNA was isolated from snap-frozen cells stored at –80°C using the Zymo Direct-zol RNA MiniPrep with TRI Reagent (Zymo Research) according to the manufacturer's protocol with the following modifications: (a) snap-frozen cells were lysed in at least 125 μl of TRI Reagent without thawing cells and (b) cells were centrifuged to collect debris or DNaseI-treated before applying to column. All samples were eluted in 25 μl of DNase/RNase-Free water. The concentration of RNA was determined using a NanoDrop 1000 (Thermo Fisher Scientific). The integrity of the RNA was determined using Agilent RNA 6000 Nano chip (Agilent Technologies). RNA samples were concentrated at room temperature using an Eppendorf Vacufuge 5301 (Eppendorf) until samples were 5 μl in volume for the array analyses. RNA was stored at –80°C before analysis.

RNA isolation and analysis for relative gene expression. RNA was isolated from snap-frozen cells stored at –80°C using the Zymo Direct-zol RNA MiniPrep with TRI Reagent according to the manufacturer's protocol with the following modifications. Snap-frozen cells were lysed in at least 125 μl of TRI Reagent without thawing cells. Cells were not centrifuged to collect debris or DNaseI treated before applying to column. All samples were eluted in 25 μl of DNase/RNase-Free water. Concentrations of the RNA samples were determined with a NanoDrop 1000 (Thermo Fisher Scientific). SuperScript IV RT (Thermo Fisher Scientific) was used for cDNA synthesis and digital droplet PCR reaction setup using ddPCR supermix for probes (no dUTP) (Bio-Rad) according to the manufacturer's protocol. Mouse *Mmp12* HEX ddPCR primers and probe were used in PCR reactions (Bio-Rad; 10042961). Droplets formed on Bio-Rad QX100 droplet generator per manufacturer's protocol. The reactions then transferred to a 96-well PCR plate (Bio-Rad) and standard thermocycling conditions were run on a SimpliAmp Thermal Cycler (Thermo Fisher Scientific). PCR droplet reactions were then analyzed with a Bio-Rad QX100 Bio-Rad droplet reader and analyzed with QuantaSoft Analysis Pro software (Bio-Rad).

mRNA profiling and data analysis and statistics. Expression of mRNA transcripts from Tregs isolated from lungs without injury (lung control), lungs at day 7 after LPS, and spleens at day 7 after LPS was profiled using the Affymetrix MoGene ST v2.1 microarrays performed by the UNC School of Medicine Functional Genomics Core Facility (n = 3 replicates in each condition).

Normalized gene expression was derived from microarray CEL files using Affymetrix Power Tools (https://media.affymetrix.com/support/developer/powertools/changelog/index.html) and custom meta-probe set mappings based on ENSEMBL v91 gene annotation. Specifically, Affymetrix probe sets were consolidated to ENSEMBL gene identifiers, and signals of probes from the CEL files were summarized to gene level using median polish, after RMA background adjustment, GC content correction, and quantile normalization, before $\log_2$ transformation. The normalized transcript expression data were used in PCA and clustering analysis and as input to Bioconductor R package, limma, for differential expression analysis by linear models (23, 24). Differentially expressed transcripts were filtered as FDR < 0.05 and fold change > 2. For GSEA, the ROAST available from limma were used (27).

Accession code. The microarray data have been deposited into the Gene Expression Omnibus (http://www.ncbi.nlm.nih.gov/geo/) as series GSE104088.

Statistics. Data other than gene or transcript expression were compared between conditions using Student t tests, Mann-Whitney rank sum test or 1-way ANOVA with Tukey's multiple comparison test between conditions. Data are expressed as the mean ± SEM. Statistical analysis was performed using GraphPad Prism 7 software. Statistical difference was accepted at $P < 0.05$.

Study approval. Procedures were conducted using protocols approved by the UNC Animal Care and Use Committee.

Author contributions

CFD, HD, JCG, CMD, and J.R. Mock conceived and designed experiments; CFD, HD, MKT, DLN, and J.R. Mock performed experiments and analysis; and CFD, HD, MKT, DLN, JCG, J.R. Martin, RSH, CMD, and J.R. Mock wrote the manuscript and provided creative input.

Acknowledgments

The authors thank the UNC Flow Cytometry Core Facility and Evan Trudeau for assistance with cell sorting and Michael J. Vernon and the UNC School of Medicine Functional Genomics Core Facility for microarray processing. The UNC Flow Cytometry Core Facility is supported in part by P30 CA016086 Cancer Center Core Support Grant to the UNC Lineberger Comprehensive Cancer Center. The Venn diagram was constructed with software from the Pacific Northwest National Laboratory (PNNL; https://omics.pnl.gov/). The *Sik1*$^{-/-}$ mouse strain used for this research project was generated by the trans-NIH Knock-Out Mouse Project (KOMP) and obtained from the KOMP Repository (www.komp.org). NIH grants to Velocigene at Regeneron Inc (U01HG004085) and the CSD Consortium (U01HG004080) funded the generation of gene-targeted ES cells for 8,500 genes in the KOMP program and archived and distributed by the KOMP Repository at UC Davis and Children's Hospital Oakland Research Institute (CHORI; U42RR024244). The authors thank the UNC Mutant Mouse Resource and Research Center (U42OD010924) and specifically Jane Hoel for cryorecovery of the *Sik1*$^{-/-}$ strain. Research was supported by the Parker B. Francis Fellowship Program (J.R. Mock) and the National Heart, Lung, and Blood Institute of the NIH: K12HL119998 (CMD), R01 HL114388 (CMD), K08HL129075 (J.R. Mock), and R03HL145255 (J.R. Mock).

Address correspondence to: Claire M. Doerschuk, Professor of Medicine and Pathology, University of North Carolina, Marsico Hall 7205, CB #7248, Chapel Hill, North Carolina 27599-7248, USA. Phone: 919.966.1782; Email: cmd@med.unc.edu.

1. Yamamoto K, et al. Type I alveolar epithelial cells mount innate immune responses during pneumococcal pneumonia. *J Immunol*. 2012;189(5):2450–2459.
2. Mizgerd JP. Respiratory infection and the impact of pulmonary immunity on lung health and disease. *Am J Respir Crit Care Med*. 2012;186(9):824–829.
3. Bhattacharya J, Matthay MA. Regulation and repair of the alveolar-capillary barrier in acute lung injury. *Annu Rev Physiol*. 2013;75:593–615.
4. Thompson BT, Chambers RC, Liu KD. Acute Respiratory Distress Syndrome. *N Engl J Med*. 2017;377(6):562–572.
5. Huynh ML, Fadok VA, Henson PM. Phosphatidylserine-dependent ingestion of apoptotic cells promotes TGF-beta1 secretion and the resolution of inflammation. *J Clin Invest*. 2002;109(1):41–50.
6. Kieran NE, Maderna P, Godson C. Lipoxins: potential anti-inflammatory, proresolution, and antifibrotic mediators in renal disease. *Kidney Int*. 2004;65(4):1145–1154.
7. Savill J. Apoptosis in resolution of inflammation. *J Leukoc Biol*. 1997;61(4):375–380.
8. Serhan CN, Savill J. Resolution of inflammation: the beginning programs the end. *Nat Immunol*. 2005;6(12):1191–1197.
9. Shevach EM. CD4+ CD25+ suppressor T cells: more questions than answers. *Nat Rev Immunol*. 2002;2(6):389–400.
10. Shevach EM. From vanilla to 28 flavors: multiple varieties of T regulatory cells. *Immunity*. 2006;25(2):195–201.
11. Mock JR, et al. Foxp3+ regulatory T cells promote lung epithelial proliferation. *Mucosal Immunol*. 2014;7(6):1440–1451.
12. D'Alessio FR, et al. CD4+CD25+Foxp3+ Tregs resolve experimental lung injury in mice and are present in humans with acute lung injury. *J Clin Invest*. 2009;119(10):2898–2913.
13. Arpaia N, et al. A Distinct Function of Regulatory T Cells in Tissue Protection. *Cell*. 2015;162(5):1078–1089.
14. Burzyn D, et al. A special population of regulatory T cells potentiates muscle repair. *Cell*. 2013;155(6):1282–1295.
15. Adamzik M, et al. An increased alveolar CD4 + CD25 + Foxp3 + T-regulatory cell ratio in acute respiratory distress syndrome is associated with increased 30-day mortality. *Intensive Care Med*. 2013;39(10):1743–1751.
16. Dial CF, Tune MK, Doerschuk CM, Mock JR. Foxp3+ Regulatory T Cell Expression of Keratinocyte Growth Factor Enhances Lung Epithelial Proliferation. *Am J Respir Cell Mol Biol*. 2017;57(2):162–173.
17. Rojas M, Woods CR, Mora AL, Xu J, Brigham KL. Endotoxin-induced lung injury in mice: structural, functional, and biochemical responses. *Am J Physiol Lung Cell Mol Physiol*. 2005;288(2):L333–L341.
18. Su X, Looney MR, Gupta N, Matthay MA. Receptor for advanced glycation end-products (RAGE) is an indicator of direct lung injury in models of experimental lung injury. *Am J Physiol Lung Cell Mol Physiol*. 2009;297(1):L1–L5.
19. Hernandez AL, et al. Sodium chloride inhibits the suppressive function of FOXP3+ regulatory T cells. *J Clin Invest*. 2015;125(11):4212–4222.
20. Zhao H, Liao X, Kang Y. Tregs: Where We Are and What Comes Next? *Front Immunol*. 2017;8:1578.
21. Vignali DA, Collison LW, Workman CJ. How regulatory T cells work. *Nat Rev Immunol*. 2008;8(7):523–532.
22. Haribhai D, Lin W, Relland LM, Truong N, Williams CB, Chatila TA. Regulatory T cells dynamically control the primary immune response to foreign antigen. *J Immunol*. 2007;178(5):2961–2972.

23. Ritchie ME, et al. limma powers differential expression analyses for RNA-sequencing and microarray studies. *Nucleic Acids Res*. 2015;43(7):e47.
24. Phipson B, Lee S, Majewski IJ, Alexander WS, Smyth GK. ROBUST HYPERPARAMETER ESTIMATION PROTECTS AGAINST HYPERVARIABLE GENES AND IMPROVES POWER TO DETECT DIFFERENTIAL EXPRESSION. *Ann Appl Stat*. 2016;10(2):946–963.
25. Smyth GK. Linear models and empirical bayes methods for assessing differential expression in microarray experiments. *Stat Appl Genet Mol Biol*. 2004;3:Article3.
26. Ashburner M, et al. Gene ontology: tool for the unification of biology. The Gene Ontology Consortium. *Nat Genet*. 2000;25(1):25–29.
27. Wu D, Lim E, Vaillant F, Asselin-Labat ML, Visvader JE, Smyth GK. ROAST: rotation gene set tests for complex microarray experiments. *Bioinformatics*. 2010;26(17):2176–2182.
28. Harada Y, et al. Metabolically programmed quality control system for dolichol-linked oligosaccharides. *Proc Natl Acad Sci USA*. 2013;110(48):19366–19371.
29. Kim JM, Rasmussen JP, Rudensky AY. Regulatory T cells prevent catastrophic autoimmunity throughout the lifespan of mice. *Nat Immunol*. 2007;8(2):191–197.
30. Misharin AV, Morales-Nebreda L, Mutlu GM, Budinger GR, Perlman H. Flow cytometric analysis of macrophages and dendritic cell subsets in the mouse lung. *Am J Respir Cell Mol Biol*. 2013;49(4):503–510.
31. Lombardi MS, Gilliéron C, Dietrich D, Gabay C. SIK inhibition in human myeloid cells modulates TLR and IL-1R signaling and induces an anti-inflammatory phenotype. *J Leukoc Biol*. 2016;99(5):711–721.
32. Darling NJ, Toth R, Arthur JS, Clark K. Inhibition of SIK2 and SIK3 during differentiation enhances the anti-inflammatory phenotype of macrophages. *Biochem J*. 2017;474(4):521–537.
33. He N, et al. Metabolic control of regulatory T cell (Treg) survival and function by Lkb1. *Proc Natl Acad Sci USA*. 2017;114(47):12542–12547.
34. Pandiyan P, Zheng L, Lenardo MJ. The molecular mechanisms of regulatory T cell immunosuppression. *Front Immunol*. 2011;2:60.
35. Wing JB, Sakaguchi S. Multiple treg suppressive modules and their adaptability. *Front Immunol*. 2012;3:178.
36. Caridade M, Graca L, Ribeiro RM. Mechanisms Underlying CD4+ Treg Immune Regulation in the Adult: From Experiments to Models. *Front Immunol*. 2013;4:378.
37. Zemmour D, Zilionis R, Kiner E, Klein AM, Mathis D, Benoist C. Single-cell gene expression reveals a landscape of regulatory T cell phenotypes shaped by the TCR. *Nat Immunol*. 2018;19(3):291–301.
38. Sullivan JM, Höllbacher B, Campbell DJ. Cutting Edge: Dynamic Expression of Id3 Defines the Stepwise Differentiation of Tissue-Resident Regulatory T Cells. *J Immunol*. 2019;202(1):31–36.
39. McClendon J, et al. Hypoxia-Inducible Factor 1α Signaling Promotes Repair of the Alveolar Epithelium after Acute Lung Injury. *Am J Pathol*. 2017;187(8):1772–1786.
40. Davey A, McAuley DF, O'Kane CM. Matrix metalloproteinases in acute lung injury: mediators of injury and drivers of repair. *Eur Respir J*. 2011;38(4):959–970.
41. Marchant DJ, et al. A new transcriptional role for matrix metalloproteinase-12 in antiviral immunity. *Nat Med*. 2014;20(5):493–502.
42. Bellac CL, et al. Macrophage matrix metalloproteinase-12 dampens inflammation and neutrophil influx in arthritis. *Cell Rep*. 2014;9(2):618–632.
43. Dufour A, et al. C-terminal truncation of IFN-γ inhibits proinflammatory macrophage responses and is deficient in autoimmune disease. *Nat Commun*. 2018;9(1):2416.
44. Morikawa H, et al. Differential roles of epigenetic changes and Foxp3 expression in regulatory T cell-specific transcriptional regulation. *Proc Natl Acad Sci USA*. 2014;111(14):5289–5294.
45. Singer BD, et al. Regulatory T cell DNA methyltransferase inhibition accelerates resolution of lung inflammation. *Am J Respir Cell Mol Biol*. 2015;52(5):641–652.
46. Bostick M, Kim JK, Estève PO, Clark A, Pradhan S, Jacobsen SE. UHRF1 plays a role in maintaining DNA methylation in mammalian cells. *Science*. 2007;317(5845):1760–1764.
47. Obata Y, et al. The epigenetic regulator Uhrf1 facilitates the proliferation and maturation of colonic regulatory T cells. *Nat Immunol*. 2014;15(6):571–579.
48. Li Q, et al. Critical role of histone demethylase Jmjd3 in the regulation of CD4+ T-cell differentiation. *Nat Commun*. 2014;5:5780.
49. Manna S, et al. Histone H3 Lysine 27 demethylases Jmjd3 and Utx are required for T-cell differentiation. *Nat Commun*. 2015;6:8152.
50. Berdeaux R, et al. SIK1 is a class II HDAC kinase that promotes survival of skeletal myocytes. *Nat Med*. 2007;13(5):597–603.
51. Singer BD. Opening the Regulatory T Cell Toolbox. *Am J Respir Cell Mol Biol*. 2017;57(2):137–138.
52. Fujita Y, Kadota T, Araya J, Ochiya T, Kuwano K. Extracellular Vesicles: New Players in Lung Immunity. *Am J Respir Cell Mol Biol*. 2018;58(5):560–565.
53. Dhamne C, Chung Y, Alousi AM, Cooper LJ, Tran DQ. Peripheral and thymic foxp3(+) regulatory T cells in search of origin, distinction, and function. *Front Immunol*. 2013;4:253.
54. Tang Q, Vincenti F. Transplant trials with Tregs: perils and promises. *J Clin Invest*. 2017;127(7):2505–2512.
55. Singer BD, King LS, D'Alessio FR. Regulatory T cells as immunotherapy. *Front Immunol*. 2014;5:46.
56. Shipley JM, Wesselschmidt RL, Kobayashi DK, Ley TJ, Shapiro SD. Metalloelastase is required for macrophage-mediated proteolysis and matrix invasion in mice. *Proc Natl Acad Sci USA*. 1996;93(9):3942–3946.
57. Valenzuela DM, et al. High-throughput engineering of the mouse genome coupled with high-resolution expression analysis. *Nat Biotechnol*. 2003;21(6):652–659.